Multiscale Integration Hybrid Algorithms for Homogeneous–Heterogeneous Reactors

D. G. Vlachos
Dept. of Chemical Engineering, University of Massachusetts at Amherst, Amherst, MA 01003

Despite many available models at different reactor length scales, no models exist for designing homogeneous–heterogeneous reactors from first principles by linking molecular with macroscopic scales. Hybrid algorithms, based on a domain decomposition method, are proposed to couple a continuum fluid-phase transport/reaction model with a new efficient, real-time surface Monte Carlo model suitable for stiff problems. These algorithms properly treat surface heterogeneities and morphology and provide the exact boundary condition to the continuum fluid-phase model. In this way, molecular-scale information is integrated into a macroscopic chemical system. The methods are applied at atmospheric pressure to a stagnant boundary layer near a catalytic surface where heterogeneities are caused by adsorbate–adsorbate interactions. Both steady-state and transient simulations are performed. Such numerical methods have the potential for microscopic control of chemical processes through macroscopic control of experimental parameters. Applications to homogeneous–heterogeneous processes such as catalytic reactors, control of morphology of solid materials with atomic resolution, and corrosion processes are also discussed.

Introduction

Homogeneous–heterogeneous processes are encountered in many technologically important areas including catalysis, materials growth and processing, electrochemistry, and corrosion. Such systems involve transport of reactants and products in a fluid boundary layer, homogeneous reactions in the fluid phase, and heterogeneous reactions on a surface, as shown in Figure 1a. It has usually been assumed that surfaces are spatially homogeneous. However, in reality all surfaces are heterogeneous due to defects, facets, reconstructions, impurities, and lateral interactions between adsorbates. Inclusion of such spatial heterogeneous features is central to improving the modeling of homogeneous–heterogeneous processes. For example, lateral interactions cause variations in macroscopic properties such as heats of adsorption, phase transitions, and pattern formation on surfaces, which are essential processes in nucleation, by which crystal growth proceeds. Thus, molecular-based phenomena control selectivities and conversion of chemical processes and solids morphology in materials fabrication. As a result, *molecular-type phenomena can strongly be manifested in macroscopic-size systems.*

A major challenge in modeling of macroscopic-size chemical systems is that elementary processes encompass a wide range of length and time scales. As an example, transport and reaction processes in a fluid boundary layer occur often in the millimeter to centimeter scales. On the other hand, length scales on a surface range from atomic dimensions for individual atoms, small catalyst particles, and point defects, to micrometer scale for facets and interstep distance in thin-film growth, to centimeter scale for a wafer of a semiconductor or a ceramic film. The corresponding time scales also vary by many orders of magnitude. The disparity of scales necessitates use of a different approach at each scale for solving such problems.

In particular, the conservation equations in a fluid phase for large length scales (compared to the mean free path of molecules) are based on the *continuum hypothesis* and have their foundations in the pioneer work of Bird, Stewart, and Lightfoot on transport phenomena (Bird et al., 1960). Nowadays, computational fluid dynamics simulators with relatively simple chemistry are routinely used. On the other hand, fluid mechanics–multicomponent transport-detailed chemistry

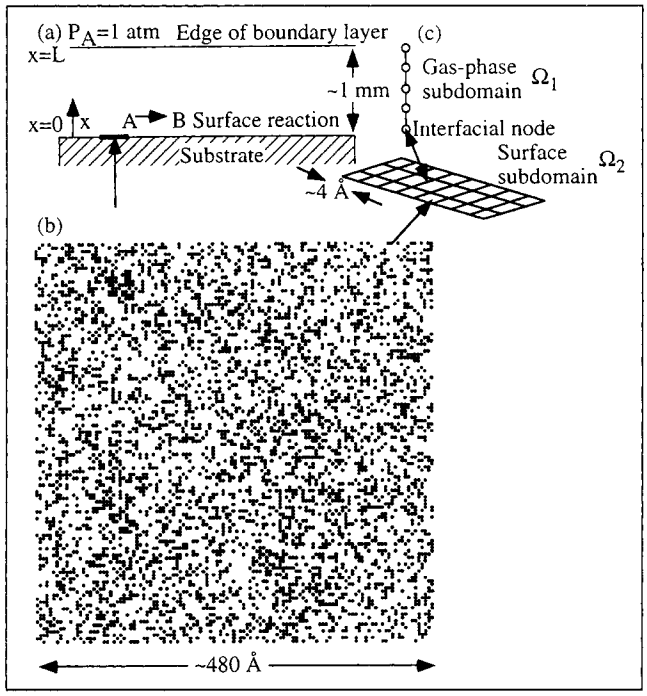

Figure 1. Physical model and computational subdomains.

(a) The reactor model consisting of a boundary layer near a reacting surface. (b) A snapshot in magnification of the surface at steady state for the simulations corresponding to Figures 5 and 6. From a macroscopic length scale, the surface appears spatially homogeneous. However, from a molecular length scale, the surface is inhomogeneous consisting of clusters of various sizes. (c) The gas-phase and surface subdomains used in the computations. The circles denote nodes (only a few are depicted), and the centers of the squares on the lattice are chemisorption sites.

models for homogeneous–heterogeneous systems are relatively scarce (with the expections of microelectronics processes (Titrowidjodjo and Pollard, 1988; Coltrin and Kee, 1989; Mountziaris and Jensen, 1991), and more recently combustion processes (Bui et al., 1996; Vlachos, 1996; Vlachos and Bui, 1996)) and limited mostly to one-dimensional geometries and exclusively to laminar flows.

The desire to design and control large-scale chemical processes from an understanding of molecular-based phenomena (Allen and Tildesley, 1989; Westmoreland and Cox, 1994; Lerou and Ng, 1996; Villermaux, 1996), and thus from first principles, and to microfabricate new materials with atomic resolution, has led to extensive *molecular length scales* simulations in recent years. As a younger approach to engineering problems, molecular modeling is less mature compared to that of macroscopic length scales. Molecular modeling involves mainly Monte Carlo (MC), molecular dynamics (MD), and quantum mechanical calculations. MC and MD simulations, used first extensively in equilibrium problems (Binder, 1986; Allen and Tildesley, 1989), are more recently being applied to reacting systems such as irreversible catalytic processes and materials processing (van der Eerden et al., 1978; Ziff et al., 1986; Madhukar and Ghaisas, 1988; Vlachos et al., 1990, 1991, 1993; Baskes et al., 1992; Catlow et al., 1994; Chuan Kang and Winberg, 1995). These simulations are the only exact way to study molecular phenomena for cases where interatomic

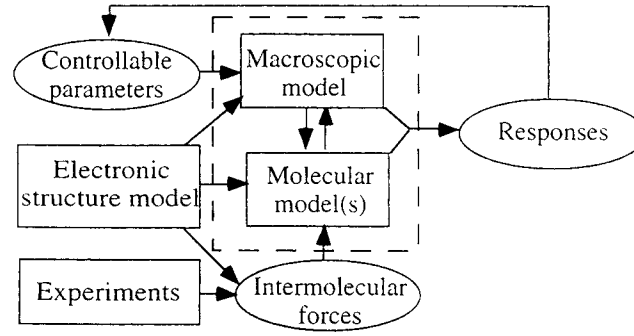

Figure 2. Integration of multiple scales in homogeneous–heterogeneous processes.

Electronic structure simulations provide interatomic potentials, thermophysical data, and kinetics data needed in molecular simulations of surfaces and continuum models of a fluid phase. Double arrows indicate the intrinsic coupling between the surface microprocesses and the continuum model. This article focuses on the integration of multiple scales between heterogeneous surfaces and a transport/reaction model in an adjacent fluid phase shown in the dashed box.

interactions, defects, impurities, and finite-size effects are important.

At present, there is no link between microscopic scales and macroscopic scales of homogeneous–heterogeneous processes. Thus, despite the fact that most applications involve relatively high pressures, so far all molecular simulations on homogeneous–heterogeneous systems have been applied to vacuum conditions (a pressure gap), where the fluid phase can be ignored. On the other hand, all continuum-level simulations have assumed that surfaces are spatially homogeneous (Kevrekidis et al., 1984; Lombardo and Bell, 1991) (a mean-field approach). Due to the disparity of length and time scales involved, a first-principles brute-force simulation of an entire system is beyond the capabilities of current supercomputers. Consequently, it is not currently known how to link the information between various scales, especially when scales are strongly coupled, as shown in Figure 2.

Here we demonstrate for the first time multiscale integration hybrid (MIH) algorithms that link molecular simulations for a surface with a macroscopic process model. To integrate multiple length scales, we have employed a domain decomposition method, where the system is partitioned into two partially overlapping subdomains, shown in Figure 1c, of different length scales. Our primary focus in this article is to assess the numerical feasibility of MIH algorithms by studying a model system of a unimolecular surface reaction, with adsorbate–adsorbate interactions, coupled with transport in an adjacent boundary layer.

Physical Model and Chemistry

The physical model considers a stagnant film of thickness L through which species A diffuses and possibly reacts by a homogeneous reaction. When species A reaches the surface, it reacts by a surface reaction (a homogeneous–heterogeneous process). The product B formed on the surface desorbs into the gas phase and is transported by diffusion away from the surface. The reactor configuration, illustrated in Figure 1a, has served as a prototype for research and teach-

ing in transport phenomena and reactor design courses (see, for example, the work of Amundson and coworkers, and Aris and coworkers (Aris and Varma, 1980; Song et al., 1991)). For simplicity, isothermal conditions are assumed.

The surface-reaction model considers adsorption of species A onto the surface and desorption of the adsorbed species AS from the surface

$$A + S \rightarrow AS \tag{1}$$

$$AS \rightarrow A + S, \tag{2}$$

where S denotes a vacant site. AS is converted into product B by a first-order surface reaction

$$AS \rightarrow B + S. \tag{3}$$

The desorption of B is taken to be very fast compared to the rest of the steps, and thus, adsorbed BS is not explicitly treated in the model. Lateral interactions also exist between species AS, resulting in the formation of clusters (spatial inhomogeneities). This is the case in many catalytic systems, as happens, for example, in the CO oxidation on platinum. Thus, this surface-reaction model has been a prototype of more complex reaction schemes (Kevrekidis et al., 1984; Vlachos et al., 1990, 1991; Lombardo and Bell, 1991). In the case of microelectronics processes, atoms of solid participate as well in the surface reaction, Eq. 3.

Here, it is assumed that the probability for adsorption is independent of the local microenvironment of each site, that is, the presence of other atoms on the surface. All sites of a bare surface are taken to be equivalent, that is, in the absence of attractive interactions the probabilities for desorption or reaction are site independent. Extension to include more complex cases, such as site defects, is straightforward, and we have reported such MC studies before (Vlachos et al., 1990; 1991). Thus, the adsorption, desorption, and surface-reaction processes follow Langmuir–Hinshelwood kinetics, with the exception of lateral interactions between adsorbed AS species. We should note that the bifurcation behavior of the preceding reaction system has been studied in a continuous stirred-tank reactor, using both the mean field approximation (Kevrekidis et al., 1984) and a MC method (Vlachos et al., 1990, 1992).

Continuum Fluid-Phase Transport Model

For the one-dimensional problem shown in Figure 1a, the conservation equation for species A in the fluid phase is

$$\frac{\partial C_A}{\partial t} = \frac{\partial}{\partial x}\left(D\frac{\partial C_A}{\partial x}\right) + R_A \tag{4}$$

with the following boundary conditions

$$C_A = C_{AL} \quad \text{at} \quad x = L \tag{5a}$$

$$D\frac{\partial C_A}{\partial x} = k_a C_A(1-\theta_A) - k_d f(C_{AS}, T, w_{AA}) \quad \text{at} \quad x = 0, \tag{5b}$$

where Ficks' first law has been assumed. The terms on the righthand side of Eq. 5b stand for the adsorption and desorption rates of species A. The function f describes the influence of lateral interactions on the desorption rate that deviates from Langmuir–Hinshelwood kinetics.

The conservation of surface species AS is

$$\frac{dC_{AS}}{dt} = k_a C_A(1-\theta_A) - k_d f(C_{AS}, T, w_{AA}) - k_r C_{AS}. \tag{6}$$

The adsorption rate constant is computed using the kinetic theory of ideal gases

$$k_a = s_0\sqrt{\frac{RT}{2\pi M}}\, e^{-E_a^0/RT}. \tag{7}$$

The reaction rate constant is given by conventional Arrhenius kinetics

$$k_r = k_r^0 e^{-E_r^0/RT}. \tag{8}$$

Due to attractive interactions, the activation energy for desorption increases with increasing coverage θ_A and is usually taken to be a linear function of θ_A (Lombardo and Bell, 1991). For convenience, the desorption rate constant k_d includes only the Arrhenius kinetics term

$$k_d = k_d^0 e^{-E_d^0/RT}, \tag{9}$$

and lateral interactions are taken into account in the function f (see below).

We assume a constant diffusivity and no homogeneous reactions ($R_A = 0$). By introducing the variables

$$x^* = x/L, \quad t^* = t/\tau, \quad u_A = C_A/C_{AL}, \quad \theta_A = C_{AS}/C_T,$$
$$f^* = f/C_T \quad k_a^* = k_a\tau C_{AL}/C_T, \quad k_d^* = k_d\tau,$$
$$k_r^* = k_r\tau, \quad \tau = L^2/D, \quad \omega = C_T/(LC_{AL}), \tag{10}$$

Eqs. 4–6 are put in the following dimensionless form

$$\frac{\partial u_A}{\partial t^*} = \frac{\partial^2 u_A}{\partial x^{*2}} \tag{11}$$

$$u_A = 1 \quad \text{at} \quad x^* = 1 \tag{12a}$$

$$\frac{du_A}{dx^*} = \omega[k_a^* u_A(1-\theta_A) - k_d^* f^*(\theta_A, T, w_{AA})] \quad \text{at} \quad x^* = 0 \tag{12b}$$

$$\frac{d\theta_A}{dt^*} = k_a^* u_A(1-\theta_A) - k_d^* f^*(\theta_A, T, w_{AA}) - k_r^*\theta_A. \tag{13}$$

At steady state, Eq. 11 results in a linear profile for u_A in the gas phase. Equations 11–13 are then reduced to a system of two nonlinear algebraic equations

$$u_{A0} = 1 - \omega k_r^*\theta_A \tag{14}$$

Table 1. Values of Parameters Used in the Model

Pressure [atm]	1
Sticking coefficient	0.1
E_a^0 [kcal/mol]	0
E_d^0 [kcal/mol]	13–15
E_r^0 [kcal/mol]	15–21
$k_d^0 = k_r^0$ [s^{-1}]	10^{13}
w_{AA} [kcal/mol]	0–2
Gas-phase diffusivity, D [cm^2/s]	0.1
Boundary layer thickness, L [cm]	0.1
Density of sites, C_T [sites/cm^2]	10^{15}
Molecular weight, M	2

$$k_a^* u_{A0}(1-\theta_A) - k_d^* f(\theta_A, T, w_{AA}) - k_r^* \theta_A = 0, \quad (15)$$

where u_{A0} is the gas-phase concentration adjacent to the surface. The values of parameters of the model are summarized in Table 1. The values of molecular weight, sticking coefficient, and length of boundary layer are typical values of our simulations on catalytic combustion of H_2/air mixtures (Vlachos, 1996; Bui et al., 1997).

Mean-field Lowest-level Hierarchical Surface Model

In the mean-field (MF) model, the atoms are assumed to be uniformly distributed on a surface and share the same number of neighbors. Taking the coverage as a continuous function of space, the function f^* is

$$f^* = e^{-c\theta_A w_{AA}/RT}\theta_A, \quad (16)$$

where c is the coordination of the surface (e.g., $c = 4$ for a square lattice representing the (100) surface). We have previously shown that the MF approximation, Eq. 16, cannot properly describe cluster formation, phase transition, the activation energy for desorption, and the dynamics of the surface (Vlachos et al., 1991).

For this homogeneous–heterogeneous model, the MF approximation enters into the desorption rate only. The desorption rate in turn appears in both the gas-phase boundary condition, Eq. 12b, which affects the diffusion flux at the surface, and the conservation of surface species AS by Eq. 13. The coupling between the fluid model and the surface comes from the fact that the concentration of A above the surface, u_{A0}, affects the surface microconfiguration through the adsorption term in Eq. 13, which in turn determines the coverage and adsorption/desorption rates that enter in the boundary condition, Eq. 12b.

Since we are interested in nonlinear boundary conditions, we have solved numerically the time-dependent problem, Eqs. 11–13 and 16. A second-order finite difference scheme has been employed for the discretization of the spatial operator using 100 nodes. In the interior of the domain, central finite difference has been used, and for the surface boundary condition, Eq. 12b, a three-point forward finite difference approximation has been used. The concentration at the boundary node was eliminated, and the resulting system of ordinary differential equations (method of lines) was then integrated using a first-order explicit Euler method and a second-order implicit trapezoidal method. To obtain the steady-state solution, one can use Newton's method to determine the unknowns (i.e., the concentration u_{A0} above the surface and the surface coverage θ_A) in Eqs. 14–16. In the absence of lateral interactions, an analytical steady-state solution can easily be obtained.

Monte-Carlo Highest-Level Hierarchical Surface Model

The MF approximation to f^*, Eq. 16, is the simplest assumption that has customarily been used in catalysis, and in essence, is the lowest-level hierarchical surface model. Better approximations to the function f^* are possible, by employing, for example, a quasi-chemical approximation (Lombardo and Bell, 1991). However, these methods are still semiempirical. On the other hand, given an interatomic potential based on experiments or quantum mechanical calculations (see also Figure 2), the MC method provides the exact solution to the problem (limited by finite-size effects), and use of the technique is indispensable when questions regarding materials structure, interfacial stress, defects, impurities, pattern formation, and so on, are concerned. In essence, the MC method is the highest-level hierarchical surface model. The (100) surface is modeled, and to illustrate the methods, just first-nearest-neighbor interactions are included. Simulations have been performed on a square lattice of 120×120 with periodic boundary conditions. The choice of a two-dimensional lattice, as compared to a one-dimensional lattice, is necessary in the presence of attractive interactions to preserve the correct physics regarding the existence of phase transitions.

Below, we describe first the transition probabilities and then a new efficient algorithm for lattice simulations. Dimensionless variables are used.

Transition probabilities

The adsorption transition probability per dimensionless unit time on site i is taken to be

$$\Gamma_{ai} = k_a^* u_A (1-\delta_i), \quad (17)$$

where δ_i is the occupancy-site function, which is either 1 (an occupied site) or 0 (an empty site).

At any time t^*, the spatially averaged adsorption transition probability per dimensionless unit time is

$$\bar{\Gamma}_a = k_a^* u_A \sum_{i=1}^{N_s} (1-\delta_i) = k_a^* u_A (N_s - N_A), \quad (18)$$

where N_s is the total number of surface sites, and N_A is the number of atoms A on the lattice.

The desorption transition probability per dimensionless unit time of site i is

$$\Gamma_{di} = k_d^* e^{-lc_i w_{AA}/RT}\delta_i, \quad (19)$$

where lc_i is the local coordination of site i. The value of lc_i varies between 0 (no nearest neighbors) and c (all nearest neighboring sites are occupied).

At any time t^*, the spatially averaged desorption transition probability per dimensionless unit time is

$$\bar{\Gamma}_d = k_d^* \sum_{i=1}^{N_s} e^{-lc_i w_{AA}/RT} \delta_i = k_d^* \sum_{j=0}^{c} \left(e^{-jw_{AA}/RT} N_j \right), \quad (20)$$

where N_j is the number of occupied sites with local coordination equal to j. In the MC model, the function f^* is

$$f^* = \sum_{lc_i = 0}^{c} \left(e^{-lc_i w_{AA}/RT} N_j \right) / N_s = \sum_{j=0}^{c} \left(e^{-jw_{AA}/RT} q_j \right). \quad (21)$$

The fraction of sites q_j with a certain energetic interaction is a strong function of the interatomic interactions, the temperature, the concentration above the surface, and the rest of the parameters of the model. Comparison of Eqs. 21 and 16 indicates that the MF model is a reasonable approximation in the limit of either a fully covered surface ($\theta_A \to 1$) or an empty surface ($\theta_A \to 0$). In the absence of attractive interactions, the Langmuir–Hinshelwood model is recovered, and the MF model is exact. This case will be used as a reference for validating the MIH schemes and assessing their accuracy.

The reaction transition probability per dimensionless unit time is

$$\Gamma_{ri} = k_r^* \delta_i. \quad (22)$$

At any time t^*, the spatially averaged reaction transition probability per dimensionless unit time is

$$\bar{\Gamma}_r = k_r^* \sum_{i=1}^{N_s} \delta_i = k_r^* N_A. \quad (23)$$

In the continuous time MC method (see for example (Vlachos, 1995a,b)) implemented here, the transition probabilities are computed before an event is executed. The total transition probability per dimensionless unit time is determine from the summation

$$\Gamma = \bar{\Gamma}_a + \bar{\Gamma}_d + \bar{\Gamma}_r, \quad (24)$$

and the average time between MC events is the inverse of the total transition probability per dimensionless unit time

$$\Delta t^* = 1/\Gamma. \quad (25)$$

Efficient Monte Carlo lattice simulations

Once the time has been incremented by Δt^*, an event is chosen among three possible microscopic processes—adsorption, desorption, and surface reaction—using Eqs. 18, 20, 23, 24, and a random number. Recall that the probability for adsorption on all empty sites and the probability for reaction of all occupied sites are taken to be site independent. Thus, once an adsorption or a reaction process has been selected, an empty site or an atom is respectively chosen at random, and the event is executed. In the case of desorption, the transition probability depends on the local microenvironment, that is, the number of nearest neighbors. We have introduced $(c+1)$ classes according to the number of nearest neighbors each atom AS may have. Each desorption class is selected based on its transition probability (see second summation in Eq. 20) among the $(c+1)$ possible cases using a random number. Finally, an atom is randomly chosen to be removed from the selected desorption class.

Practically, a first random number RN between 0 and 1 is computed and multiplied by Γ to convert it between 0 and the maximum possible transition probably at that instant. If $RN \le \bar{\Gamma}_a$, then an adsorption microprocess is selected, and a particular empty site is chosen at random (using a second random number) terminating the selection process. If $\bar{\Gamma}_a < RN \le \bar{\Gamma}_a + \bar{\Gamma}_d$, then desorption is selected. The interval between $\bar{\Gamma}_a$ and $\bar{\Gamma}_a + \bar{\Gamma}_d$ is partitioned in subintervals determined by the probability of each desorption class. A specific desorption class is selected based on which subinterval the random number RN falls in. After a desorption class has been selected, a second random number is used to select the specific site. If $\bar{\Gamma}_a + \bar{\Gamma}_d < RN \le \bar{\Gamma}_a + \bar{\Gamma}_d + \bar{\Gamma}_r$, a reaction microprocess is executed. The specific reaction site is again selected using a second random number among the occupied sites.

We should note that the atom coordinates, local coordination numbers, number of atoms in each class, and so on, are saved in matrices. After each MC event, the elements of these matrices are updated only locally, that is, in a small radius, depending on the distance of the interactions; for interactions between first-nearest neighbors, this includes the central atom plus its four nearest neighbors. In particular, the classes affected by a microscopic process are identified, and sites (coordinates) are subtracted from the old classes, before the even was executed, and added to new classes that sites belong to, after execution of the event. Also, the total transition probability $\Gamma(t + \Delta t)$ is updated only locally (without a computation over the entire surface), by simply subtracting the old values of the probabilities of the affected classes from $\Gamma(t)$ and adding their corresponding new values.

The update of matrices includes some overhead because of the bookkeeping and is the most complex aspect in the implementation, as compared to a conventional MC algorithm where sites are chosen at random (Ziff et al., 1986; Vlachos et al., 1991). On the other hand, such an algorithm avoids screening of the entire surface. As a result, the speed of the algorithm is independent of the lattice size, and simulations of large lattices are possible without any additional overhead. However, the time step is inversionally proportional to the number of lattice sites. Thus, for a fixed number of MC events, as the lattice size increases, the real time simulated decreases.

In instances when transition probabilities change considerably with time, such as in stiff problems, or the probability is low, such as in migration of atoms from the center of large clusters, the proposed algorithm can be computationally more efficient than a conventional MC algorithm (Ziff et al., 1986; Vlachos et al., 1991) by several orders of magnitude. Part of this speedup comes from the fact that all events are successful, and part because events with a low probability are infrequently chosen instead of being chosen completely at random. In fact, in many cases, the proposed MC algorithm makes simulations of long real time feasible. This is espe-

cially the case for MIH models where multiple time scales are involved. In addition, real time is included in the simulations so that proper coupling with the gas-phase transport model is possible.

Domain Decomposition Methods for Steady-state Solutions

Domain decomposition methods have attracted considerable attention in the solution of partial differential equations (Chan, 1988; Keyes et al., 1991). These methods have been developed for problems encountered in generating grids in complex configurations. Such methods are designed to provide computational efficiency by either simplifying grid generation through subdivision of the flow domain in subdomains with an easily constructed grid, or employment of different numerical schemes in different subdomains, or use of a different form of flow equation in different subdomains. An example of the latter case involves use of Euler vs. Navier–Stokes equation for fast flows, depending on the distance from a wall (Canuto and Russo, 1994).

Here, we use a domain-decomposition method that differs from previous work, in the sense that different numerical algorithms (a stochastic one and a deterministic one) are used in each subdomain required by local inhomogeneities found on the surface due to molecular interactions. Furthermore, the dimensionality and scales of the two subdomains used, one for the gas-phase (Ω_1) and one for the surface (Ω_2) shown in Figure 1c, differ. Ω_2 is two-dimensional to preserve the correct physics. Spatially averaged properties in Ω_2 are used in the interfacial node of Ω_1 (a one-dimensional subdomain) from which the surface appears as spatially homogeneous due to the large difference in length scales (see Figure 1b). The length scale over which spatial surface nonuniformities are important is related to the correlation length, and a sufficiently large simulation box is needed in molecular simulations to properly describe such heterogeneities. There are two variations of the methodology that are described next.

Parametrization of boundary conditions

The surface microprocesses are simulated using the MC algorithm for different gaseous concentrations of reactants, products, and intermediates. Such simulations provide steady-state spatially averaged quantities of interest such as cluster-size distributions, coverages, and rates needed in the mass-transfer boundary conditions (here just the function f^*). Subsequently, these quantities are fitted to compute analytical functions vs. concentrations that are then inserted into the boundary conditions of the mass-transfer problem (e.g., here in Eqs. 14 and 15). In this way, one can compute the steady-state solution of the process.

This method is applicable only to steady-state problems, and when a multicomponent system is employed, fitting is needed in a multidimensional parameter space through factorial design. A good guess of concentrations above the surface is important so that parametrization is done within the window of operation. When spatially averaged surface quantities are multivalued functions of the fluid concentration, one could in principle parametrize each stable branch and use multiple boundary conditions over the regime of multiplicity for solving the full problem. It is anticipated, though, that use of a few points for fitting may result in missing such bifurcation phenomena, so special care is needed when such a method is used. The method is graphically illustrated in the following examples and was not pursued further because the following iterative scheme was found to be superior.

Iterative scheme

In this algorithm, an initial concentration above the surface u_{A0} and an initial microconfiguration are guessed, and a MC simulation is performed in Ω_2. Note that the choice of the initial microconfiguration in the first iteration affects only the time needed to reach steady state. After steady state has been reached in MC simulations (see below), the molecular-based spatially and temporally averaged rates—the rates of adsorption, desorption, surface reaction–are determined over a certain time interval. These rates (specifically the function f^* in this model) are then inserted into the surface boundary condition, for example, Eq. 12b. The steady-state fluid-phase problem is next solved in Ω_1, giving the species profiles across the boundary layer and the unknown concentrations just above the surface. Due to the linearity of the gas-phase problem, one can directly use Eq. 14 for this model. The concentrations above the surface are subsequently used in a new MC simulation for the next iteration. The iterations of the MIH scheme are continued until convergence of the overall algorithm has been achieved, or up to a maximum number of iterations. The iterative MIH scheme is illustrated in Figure 3. We should note that this iterative scheme resembles the "Zanolli" patching scheme used for different discretizations of continuum equations on two different subdomains (Henderson and Karniadakis, 1991).

Steady-state criteria have been implemented in MC simulations and applied at each iteration of the MIH scheme. In particular, the time average of the normalized residual of the surface species conservation

$$r_i = \int_{t_i^*}^{t_{i+1}^*} \left(\bar{\Gamma}_a - \bar{\Gamma}_d - \bar{\Gamma}_r\right) dt^* / \int_{t_i^*}^{t_{i+1}^*} \bar{\Gamma}_a \, dt^* \qquad (26)$$

was evaluated over specified intervals of time ($t_{i+1}^* - t_i^*$) (in fact, a discrete version of Eq. 26 was used). Steady state was assumed if, first, the residual became lower than some prespecified tolerance (a tolerance criterion) and if, second, the normalized residual started fluctuating with time around zero (an inflection criterion). Time averages of molecular-based rates were computed after these criteria were met and subsequently inserted in the boundary condition, Eq. 12b, for the next iteration.

As usually happens with nonlinear systems, there is no guarantee that convergence can be obtained by employing an iterative method. In addition, the number of iterations needed may be too large, resulting in low computational speed. Also, the role of fluctuations of the molecular model in the convergence of the overall scheme is difficult to predict *a priori*. We have addressed these issues through numerical experimentation on the model system considered here, and we discuss these issues next.

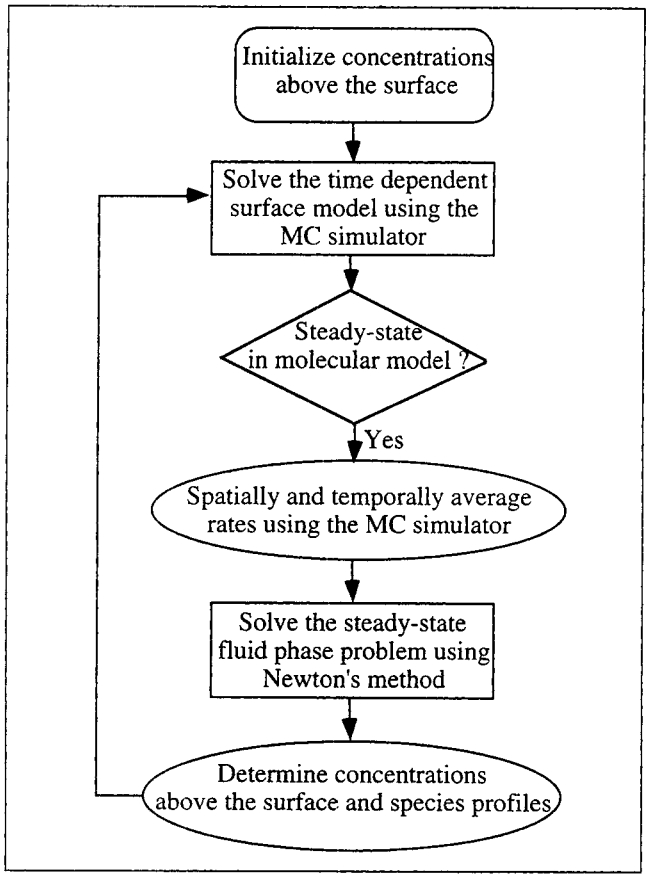

Figure 3. Iterative MIH algorithm proposed for computing steady-state solutions of homogeneous–heterogeneous systems in the presence of a heterogeneous surface.

The algorithm is terminated after a certain number of iterations or after convergence criteria have been met.

Illustrative examples and comparison of methods

We first consider an example where attractive interactions are zero so that the MIH algorithms can be validated. The solid lines in Figure 4b show the reaction isotherm, Eq. 15, and transport, Eq. 14, obtained by MC simulations. The intersection of the two curves determines graphically the steady-state solution computed by the parametrization of the boundary-conditions method.

Results from the iterative MIH algorithm are shown in Figure 4a, where the coverage and gas-phase concentration u_{A0} adjacent to the surface are plotted vs. the number of iterations for two initial gas-phase concentrations u_{A0} indicated, starting with a clean surface at the beginning of each simulation. The steady-state solution is obtained in a relatively small number of iterations. Convergence has been obtained for all other initial guesses attempted with a similar number of iterations. At each iteration, we have typically used 10^5 MC events. A number of these MC events has been discarded at the beginning of each iteration to eliminate the transient caused by a change in the gas-phase concentration. The results shown in Figure 4a can also be plotted in a phase portrait of θ_A vs. u_{A0}. In such a plot, the trajectories from all different initial guesses coincide on a single curve that is a certain section of the reaction isotherm. The points in Figure 4b show two examples corresponding to simulations of Figure 4a. Different trajectories are attracted to the same fixed point corresponding to the steady-state solution.

Concerning the accuracy of the iterative MIH scheme, the time-averaged steady-state coverage and concentration above the surface differ from the analytical exact values by less than 0.5%. This difference is excellent for these types of simulations and is within the standard deviation of simulations. In addition, the normalized residual of the surface-species conservation equation fluctuates between positive and negative values and remains of the order $O(10^{-2}-10^{-3})$. The magnitude of the normalized residual depends on the lattice size, the amplitude of fluctuations, which are a function of the parameters of the model, and the time interval over which statistics are collected. The CPU time needed to obtain the steady-state solution shown in Figure 4a is typically a couple of minutes on an SGI Indigo^2 XZ (R4400/200 MHz) workstation.

Here, the case where an unstable stationary solution is surrounded by a stable oscillatory attractor has not been examined (such parameters are currently difficult to identify for a hybrid model). However, it is expected that in such a case the method will not converge to the unstable stationary solution, that is, large fluctuations may occur whose amplitude does not decrease with increasing lattice size as happens with sta-

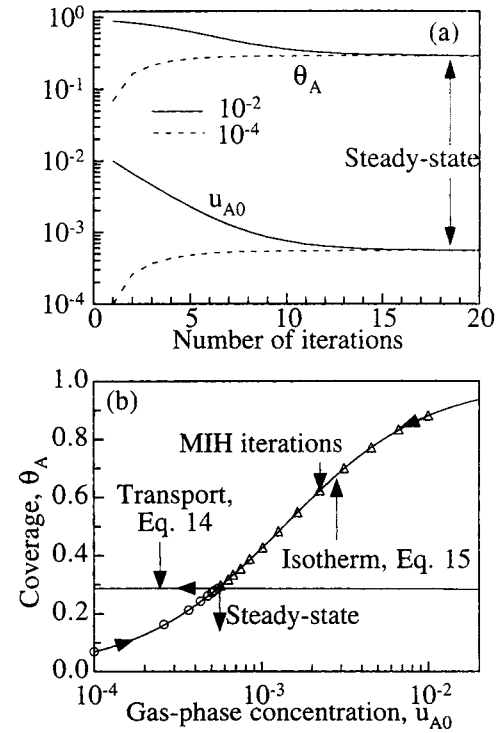

Figure 4. Domain decomposition steady-state solution in the absence of attractive interactions.

(a) The coverage and gas-phase concentration u_{A0} vs. the number of iterations for two initial guesses in u_{A0}. (b) The solid lines show the reaction isotherm and the steady-state transport, Eq. 14. The points correspond to the iterations shown in (a), and the arrows along the isotherm show the convergence toward the fixed point. The parameters are $E_d^0 = E_r^0 = 15$ kcal/mol and 400 K.

ble stationary solutions. While this is typically not a problem in deposition reactors where multiple solutions and oscillations are scarce, further research is needed in model catalytic systems to delineate such algorithmic aspects.

Next in Figure 5 we examine an example where attractive interactions are important so that the surface is spatially inhomogeneous at an atomic length scale. Figure 5a shows the coverage and gas-phase concentration adjacent to the surface vs. the number of iterations for the two initial concentrations indicated. Convergence in this example is attained in a few iterations. Figure 5b shows the reaction isotherms for the MF and MC models along with the trajectories leading to the fixed-point stationary solution. Notice that the two isotherms differ slightly for these conditions, mainly for intermediate coverages. Since θ_A, based on Eq. 14, is relatively flat over the concentration regime depicted, the steady-state coverage differs slightly between the two models. However, the gas-phase concentrations differ by ~ 12%.

The desorption rate, which is proportional to f^*, vs. the gas-phase concentration, u_{A0}, is shown for the MF model and MC model in Figure 6. It is seen that even though the isotherms do not differ significantly in Figure 5b, the desorption rates, which depend on the spatial distribution of atoms, can differ by as much as a factor of 4. This is because attractive interactions result in formation of clusters by a two-dimensional nucleation process. The surface reaction creates

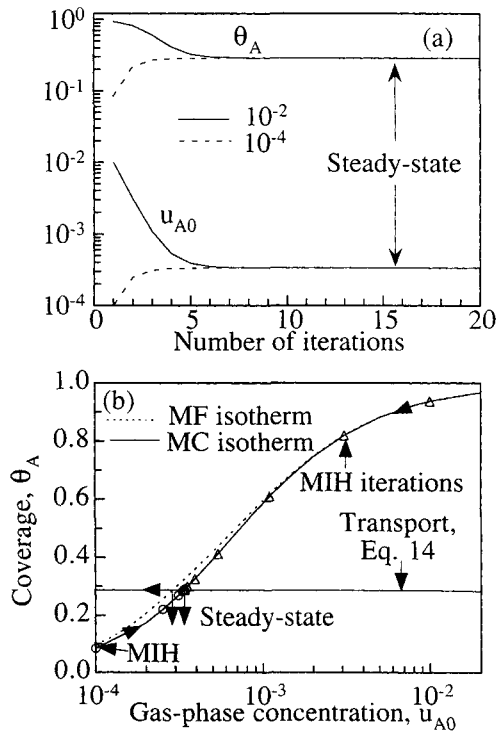

Figure 5. Domain decomposition steady-state solution in the presence of attractive interactions.

(a) The coverage and gas-phase concentration u_{A0} vs. the number of iterations in the presence of attractive interactions for two initial guesses in u_{A0}. (b) The solid lines show the reaction isotherm and the steady-state transport, Eq. 14, obtained from MC simulations. The dashed line shows the MF reaction isotherm. The points correspond to the iterations shown in (a), and the arrows along the isotherm show the convergence toward the fixed point. The parameters are $E_d^0 = E_r^0 = 15$ kcal/mol, $w_{AA} = 2$ kcal/mol, and 400 K.

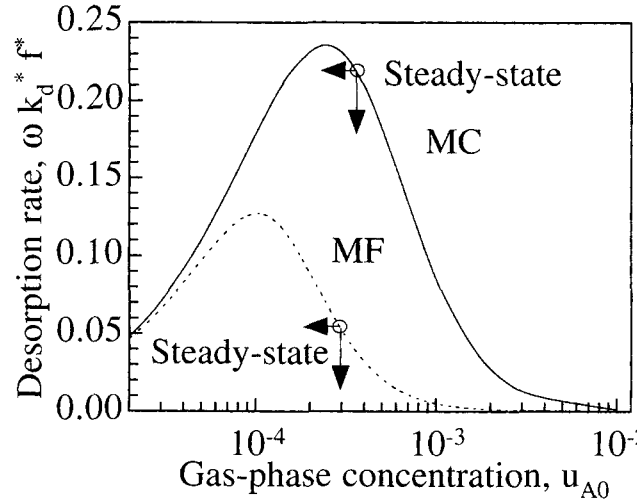

Figure 6. Desorption rate from MC and MF models vs. the gas-phase concentration u_{A0}.

The circles indicate steady-state solution. Even though isotherms differ slightly, desorption rates may differ by up to a factor of 4. The parameters correspond to Figure 5.

open sites in these clusters at random positions, resulting in a nonuniform atom distribution. An illustrative snapshot of the adatoms on the surface is shown in Figure 1b.

Using the MC desorption rate vs. coverage data (which we have taken as representative of experimental data), we have extracted the activation energy for desorption on a bare surface E_d^0 and the energy of interactions w_{AA} using the MF approximation Eq. 16. We have found that w_{AA} and E_d^0 differ from the correct values by ~ 1 kcal/mol and 0.5 kcal/mol, respectively. The error in the energy of lateral interactions is ~ 50%. This example is indicative of the important role of molecular interactions in macroscopic quantities such as activation energies and rates.

From a numerical point of view, the iterative MIH method is easily extendible to multicomponent systems, and computes only a section of the isotherm as compared to the parametrization of the boundary-conditions method. Our simulations indicate that the iterative domain decomposition scheme is robust and sufficiently accurate, and is the preferred method when a steady-state solution is of interest. When multiple steady states exist for the hybrid model, the initial guess will determine the converged solution obtained, as happens also with Newton's method.

Domain-Decomposition Fully Time-dependent Simulations

The preceding techniques may be suitable for steady-state solutions, but cannot address time-dependent situations such as the dynamics during an ignition event or when the main reactant is periodically switched, such as in growth of multilayer heterostructures. Thus, a fully coupled MIH time-dependent numerical scheme has also been implemented.

Proposed algorithm

The time-dependent MIH scheme works as follows. At some time t^*, the vector $U(t^*)$ of gas-phase concentrations

at the discretization nodes and a surface microconfiguration $\{\delta_i\}_{i=i}^{N_s}$ $[t^*, u_{A0}(t^*, f^*)]$ are considered. The spatially averaged rates are first determined over the entire surface in Ω_2 to give the function f^* (see Eq. 21). The concentration adjacent to the surface $u_{A0}(t^*)$ is then determined using the boundary condition Eq. 12b. This completes the solution $[U, u_{A0}, \{\delta_i\}]$ of the MIH model at time t^*.

The transition probabilities are then evaluated as described by Eqs. 18, 20, 23 and 24, and the next time step Δt^* is determined. Subsequently, the solution is advanced to $t^* + \Delta t^*$. In particular, an MC event is executed in Ω_2 based on the transition probabilities explained earlier, and the continuum equations are advanced in Ω_1 according to

$$\text{In } \Omega_2: \{\delta_i\}_{i=i}^{N_s}[t^*, u_{A0}(t^*, f^*)] \rightarrow \{\delta_i\}_{i=i}^{N_s}(t^* + \Delta t^*, u_{A0}) \tag{27a}$$

$$\text{In } \Omega_1: \boldsymbol{U}(t^* + \Delta t^*) = \boldsymbol{U}(t^*) + \Delta t^* \cdot \boldsymbol{F}[\boldsymbol{U}(t^*), u_{A0}(t^*, f^*)]. \tag{27b}$$

Here $\boldsymbol{F}$ is the vector of functions obtained by applying the method of lines to Eq. 11. In other words, during the time interval Δt^*, the gas-phase concentrations are advanced by an explicit Euler time-integration method using the known fluid-phase solution $\boldsymbol{U}$ and the interfacial concentration, u_{A0}, that was determined from the function f^*. In addition, the surface is advanced by the MC method using the previous microconfiguration and the concentration(s) above the surface. The concentrations determined from the boundary conditions at the new time step are used to update the transition probabilities, and a new time step begins. Note that the magnitude of the time step changes dynamically at each MC event based on current transition probabilities, that is, the atom distribution on the surface and the gaseous concentration u_{A0}.

We have observed that the requirement of satisfying the mass-transfer boundary condition at each time step induces some fluctuations into the gaseous concentration u_{A0} of species A. Even though these fluctuations propagate into the interior of the discretization domain, the small time scale of the molecular simulations leads to very smooth variation in the concentration at the rest of the nodes. In all simulations we have carried out, these fluctuations have not caused any problem. The fluctuations can be reduced by increasing the lattice size at the expense of reducing the real time simulated over the course of a simulation. The preferred method for reducing the fluctuations is to perform many MC simulations in parallel over the time interval Δt^*. At the end of each time step, a time-average rate should be computed and used in the boundary condition of the continuum model. Alternatively, one could assume that over a small time interval, the gaseous concentrations do not change. Thus, instead of updating the concentrations at each molecular event, one could update them after a certain number of MC events using molecular time-average values.

Illustrative examples

Results from MIH time-dependent simulations are shown, in the absence of attractive interactions, in Figure 7, where the dynamics is followed after an abrupt increase in temperature from 300 K to 400 K. Aside from fluctuations, the MIH simulations (solid lines) are indistinguishable from the MF model (dashed lines), which is exact in this case. For a certain period of time, the gaseous concentration decreases slowly and the surface coverage is almost constant. After a significant reduction in the gas-phase concentration, the surface responds by removing atoms through desorption and reaction to reach a steady state that is in excellent agreement with the analytical solution shown in Figure 4. The gaseous concentrations at the second and third nodes are also shown to illustrate the low amplitude of fluctuations at the rest of the gas-phase nodes.

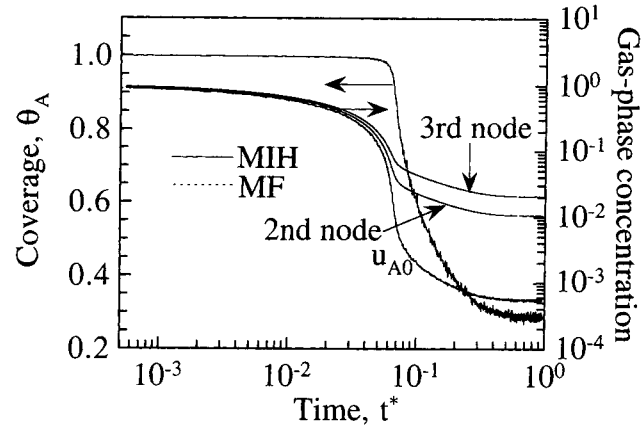

Figure 7. Domain decomposition unsteady-state solution in the absence of attractive interactions.

Time-dependent MIH simulations corresponding to an abrupt jump in temperature from 300 K to 400 K for the parameters shown in Figure 4. The amplitude of fluctuations at the noninterfacial discretization nodes is very low. The steady-state solution is in agreement with Figure 4. Aside from fluctuations, the results of the MF model are indistinguishable from the ones of the MIH model.

At atmospheric pressure, the adsorption flux is large, and the characteristic time for adsorption of an atom on an empty lattice is very short ($\sim 7\times10^{-13}$ s), compared to the gas-phase diffusion time (~ 0.1 s). Similarly, at high temperatures desorption and reaction are also fast. The surface time scales change significantly with temperature and the distribution of atoms on the surface. This disparity of time scales indicates the necessity of efficient MC simulations (a conventional algorithm we tried has never reached a steady-state solution in a reasonable CPU time). The simulation shown in Figure 7 requires a total of 2×10^9 successful MC events corresponding to ~ 18 h of CPU time on an SGI Indigo^2 XZ (R4400/200 MHz) workstation. Such a long MC simulation is due to the slow evolution of the gas phase. For this simulation, the domain-decomposition iterative MIH scheme proved much more efficient in computational time as compared to the fully time-dependent method concerning the steady-state solution.

Figure 8 shows results from MIH time-dependent simulations in the presence of attractive interactions, where the dynamics is followed after an abrupt increase in temperature from 300 K to 400 K. For these conditions, some deviations in the gas-phase concentrations are found between the MF model and the MIH model, especially at long times where most deviations between the isotherms exist. However, the overall difference is small, as expected from the slight differ-

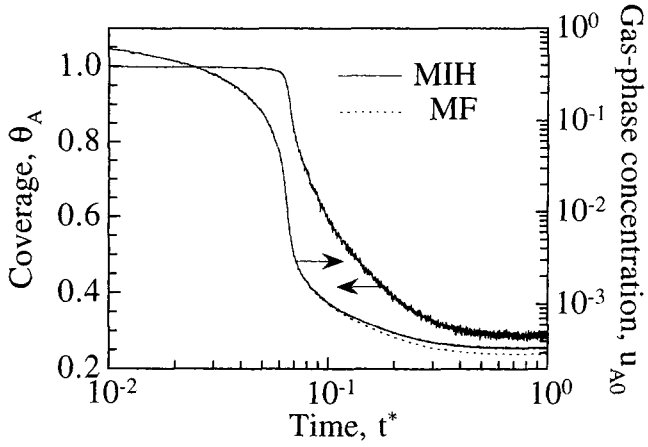

Figure 8. Domain decomposition unsteady-state solution in the presence of attractive interactions for single-valued isotherms.

Time dependent MIH and MF simulations corresponding to an abrupt jump in temperature from 300 K to 400 K for the parameters shown in Figure 5. Steady-state solution is in agreement with Figure 5. Deviations in the predictions of the gas-phase concentrations of the two models occur at long times.

ence between isotherms shown in Figure 5b. This computation took about 1 h of CPU time.

Finally, an example is considered in Figure 9 where the isotherms and dynamics between the MF and MIH models differ significantly. In the MF model, the reaction isotherm Eq. 15 exhibits multiple solutions and is intersected by the stationary transport Eq. 14 at an unstable point in Figure 9a giving rise to the periodic oscillations shown in Figure 9b. In contrast, the MC isotherm is a single-valued function (near a cusp point), and no oscillations exist, as shown in Figure 9b. Large fluctuations in θ_A and u_{A0} are found because of the proximity of the system to a cusp point (a critical point). The dynamics near cusp points has been analyzed in previous work (Vlachos et al., 1991). For example, it has been found that near cusp points there are large amplitude fluctuations whose amplitudes decrease considerably as the lattice size increases. Note, however, that even in this case, the amplitude of fluctuations in the next two discretization nodes has considerably diminished, indicating that fluctuations of a small lattice are attenuated fast in the gas phase.

The lack of oscillations in MC simulations in the preceding example is caused by nucleation of multiple clusters (local oscillators) on the surface due to attractive interactions. Due to the stochastic nature of nucleation, these multiple clusters can form at widely different times (oscillators out of phase) resulting in a spatially nonoscillating system. As a result, it appears that surface-catalyzed mean-field models usually predict a wider range over which multiple solutions and oscillations occur as compared to Monte-Carlo simulations.

Also note that in order to distinguish between fluctuations, which are inherent in Monte-Carlo simulations, and oscillations, which may be driven, for example, from kinetic interactions, one could increase the lattice size of molecular simulations. If the amplitude of dynamically varying quantities drops with increasing size (e.g., with the square root of the size as predicted by statistical mechanics for equilibrium systems),

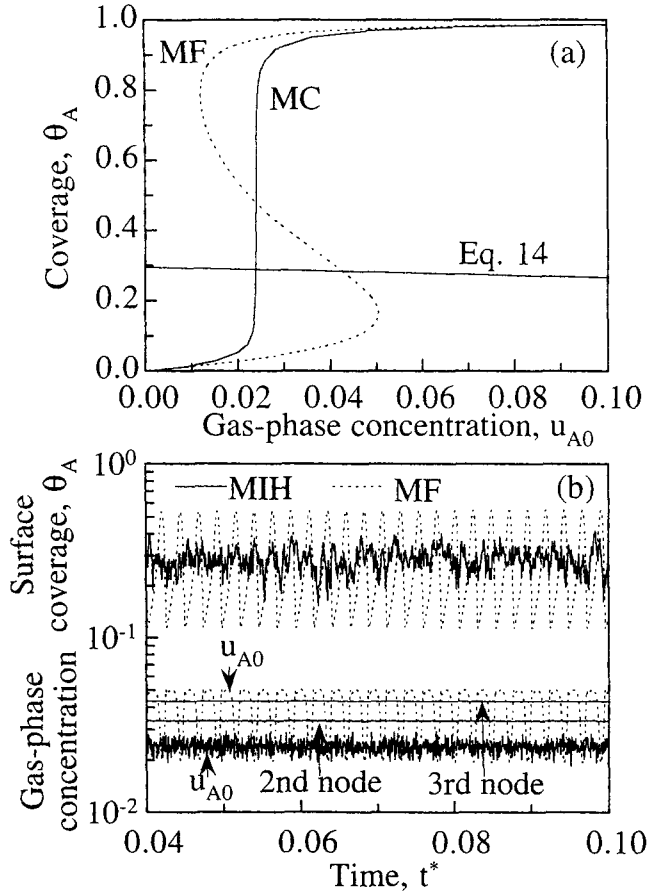

Figure 9. Domain decomposition unsteady-state solution in the presence of attractive interactions for multivalued MF isotherm.

(a) The MF isotherm (multiple-valued) and the MC isotherm (single-valued) along with the transport, Eq. 14, intersecting the isotherms at an unstable and a stable point, respectively. Time-dependent MF simulations show self-sustained oscillations, whereas MIH simulations show large fluctuations but not oscillations. The amplitude of fluctuations at the noninterfacial discretization nodes is low. The parameters are $E_d^0 = 13$ kcal/mol, $E_r^0 = 21$ kcal/mol, $w_{AA} = 2$ kcal/mol, and $T = 550$ K.

this is an indication that these variations are fluctuations in the system rather than an actual oscillatory attractor. In contrast, oscillations (period and amplitude) should not be considerably affected by lattice size. However, a decrease in fluctuations, superimposed on oscillating quantities, should be observed with increasing lattice size.

The preceding simulations have been performed on workstations. However, domain-decomposition and Monte-Carlo methods (especially statistics) can in general be parallelized. Thus, it would be desirable in future computations that parallel supercomputers or clusters of fast workstations be employed for large practical multiscale problems.

Conclusions

Multiscale integration hybrid (MIH) algorithms have been developed that combine Monte-Carlo simulations for heterogeneous surfaces with continuum transport/reaction models in an adjacent boundary layer. These algorithms are based on

a domain-decomposition technique. One class of algorithms (parametrization of boundary conditions and an iterative scheme) is applicable only to steady-state problems, whereas a second one (a fully time-dependent algorithm) is applicable to transient problems as well. The iterative MIH algorithm is computationally much more efficient compared to the fully time-dependent numerical scheme regarding steady-state solutions. A key factor in computational efficiency of the MIH schemes is due to the new efficient, real-time lattice Monte-Carlo algorithm suitable for stiff problems. Even though other similar numerical schemes may be developed in the future, an important feature of this work is the demonstration of the feasibility of such simulations at high pressures of technological relevance where time scales very significantly.

These MIH numerical schemes offer the advantage of integrating molecular-type information into macroscopic chemical processes and therefore provide an opportunity of designing and controlling chemical processes with an atomic resolution. The methods developed here were applied to a stagnant boundary layer with one catalytic surface reaction. However, these techniques can easily be applied to other areas, such as separations and materials synthesis and processing. Application of these MIH numerical schemes to real systems of technological interest is in progress.

Acknowledgment

This work was supported by a National Science Foundation Career Award under grant CTS-9702615 and an Instrumentation Award under NSF grant CTS-9410994.

Notation

C_A = gas-phase concentration of species A
C_{AL} = inlet concentration of species A
C_{AS} = surface concentration of species AS
E^0 = activation energy on a bare surface
k^0 = preexponential
R = ideal gas constant
R_A = fluid-phase chemical production rate of species A
s_0 = sticking coefficient on a clean surface
T = temperature
u_A = dimensionless concentration of species A
w_{AA} = energy of adsorbate–adsorbate interactions, Eqs. 16 and 21
x = spatial coordinate
τ = characteristic gas-phase diffusion time

Literature Cited

Allen, M. P., and D. J. Tildesley, *Computer Simulation of Liquids*, Oxford Science Publications, Oxford (1989).

Aris, R., and A. Varma, eds., *The Mathematical Understanding of Chemical Engineering Systems—Selected Papers of Neal R. Amundson*, Pergamon Press, Oxford (1980).

Baskes, M. I., R. G. Hoagland, and A. Needleman, "Summary Report: Computational Issues in the Mechanical Behavior of Metals and Intermetallics," *Mater. Sci. Eng. A*, **159**, 1 (1992).

Binder, K., ed., *Monte Carlo Methods in Statistical Physics*, Springer-Verlag, Berlin (1986).

Bird, R. B., W. E. Stewart, and E. N. Lightfoot, *Transport Phenomena*, Wiley, New York (1960).

Bui, P.-A., D. G. Vlachos, and P. R. Westmoreland, "Homogeneous Ignition of Hydrogen/Air Mixtures over Platinum," *Int. Symp. on Combustion*, The Combustion Institute, Pittsburgh, p. 1763 (1996).

Bui, P.-A., D. G. Vlachos, and P. R. Westmoreland, "Modeling Ignition of Catalytic Reactors with Detailed Surface Kinetics and Transport: Combustion of H_2/Air Mixtures over Platinum Surfaces," *Ind. Eng. Chem. Res.*, **36**(7), 2558 (1997).

Canuto, C., and A. Russo, "Self-adaptive Coupling of Mathematical Models and/or Numerical Methods," *Contemp. Math.*, **157**, 35 (1994).

Catlow, C. R. A., R. G. Bell, and J. D. Gale, "Computer Modeling as a Technique in Materials Chemistry," *J. Mater. Chem.*, **4**(6), 781 (1994).

Chan, T. F., *Domain Decomposition Algorithms and Computation Fluid Dynamics*, Research Institute for Advanced Computer Science, NASA Ames Research Center, Moffett Field, CA (1988).

Chuan Kang, H., and W. H. Winberg, "Modeling the Kinetics of Heterogeneous Catalysis," *Chem. Rev.*, **95**, 667 (1995).

Coltrin, M. E., and R. J. Kee, "A Mathematical Model of the Gas-Phase and Surface Chemistry in GaAs MOCVD," *Proc. Mater. Res. Soc.*, **145**, 119 (1989).

Henderson, R., and G. E. Karniadakis, "Hybrid Spectral Element Methods for Flows over Rough Walls," *Proc. Int. Symp. on Domain Decomposition Methods for Partial Differential Equations*, D. E. Keyes, T. F. Chan, G. Meurant, J. S. Scroggs, and R. G. Voigt, eds., SIAM, Philadelphia, p. 485 (1991).

Kevrekidis, I., L. D. Schmidt, and R. Aris, *Surf. Sci.*, **137**, 151 (1984).

Keyes, D. E., T. F. Chan, G. Meurant, J. S. Scroggs, and R. G. Voigt, eds., *Proc. Int. Symp. on Domain Decomposition Methods for Partial Differential Equations*, SIAM, Philadelphia (1991).

Lerou, J. J., and K. M. Ng, "Chemical Reaction Engineering: A Multiscale Approach to a Multiobjective Task," *Chem. Eng. Sci.*, **51**(10), 1595 (1996).

Lombardo, S. J., and A. T. Bell, "A Review of Theoretical Models of Adsorption, Diffusion, Desorption, and Reaction of Gases on Metal-Surfaces," *Surf. Sci. Rep.*, **31**(1–2), 1 (1991).

Madhukar, A., and S. V. Ghaisas, "The Nature of Molecular-beam Epitaxial-growth Examined via Computer-simulations," *CRC Crit. Rev. Solid State Mater. Sci.*, **14**, 1 (1988).

Mountziaris, T. J., and K. F. Jensen, "Gas-phase and Surface Reaction Mechanisms in MOCVD of GaAs with Trimethyl-Gallium and Arsine," *J. Electrochem. Soc.*, **138**, 2426 (1991).

Song, X., L. D. Schmidt, and R. Aris, "Steady States and Oscillations in Homogeneous-Heterogeneous Reaction Systems," *Chem. Eng. Sci.*, **46**(5/6), 1203 (1991).

Titrowidjodjo, M., and R. Pollard, "Elementary Processes and Rate-limiting Factors in MOVPE of GaAs," *J. Cryst. Growth*, **93**, 108 (1988).

van der Eerden, J. P., P. Bennema, and T. A. Cherepanova, "Survey of Monte Carlo Simulations of Crystal Surfaces and Crystal Growth," *Prog. Cryst. Growth Charact.*, **1**, 219 (1978).

Villermaux, J., "New Horizons in Chemical Engineering," World Congress of Chemical Engineering, San Diego (1996).

Vlachos, D. G., "Growth of Elongated Nanostructures," *Mater. Sci. Eng. A*, **204**(1–2), 90 (1995a).

Vlachos, D. G., "Instabilities in Homogeneous Nonisothermal Reactors: Comparison of Deterministic with Monte Carlo Simulations," *J. Chem. Phys.*, **102**(4), 1781 (1995b).

Vlachos, D. G., "Homogeneous-Heterogeneous Oxidation Reactions over Platinum and Inert Surfaces," *Chem. Eng. Sci.*, **51**(10), 2429 (1996).

Vlachos, D. G., and P.-A. Bui, "Catalytic Ignition and Extinction of Hydrogen: Comparison of Simulations and Experiments," *Surf. Sci.*, **364**(3), L625 (1996).

Vlachos, D. G., L. D. Schmidt, and R. Aris, "The Effects of Phase Transitions, Surface Diffusion, and Defects on Surface Catalyzed Reactions: Oscillations and Fluctuations," *J. Chem. Phys.*, **93**, 8306 (1990).

Vlachos, D. G., L. D. Schmidt, and R. Aris, "The Effect of Phase Transitions, Surface Diffusion, and Defects on Heterogeneous Reactions: Multiplicities and Fluctuations," *Surf. Sci.*, **249**, 248 (1991).

Vlachos, D. G., L. D. Schmidt, and R. Aris, "Spatial and Temporal Patterns in Catalytic Oscillations," *Physica A*, **188**, 302 (1992).

Vlachos, D. G., L. D. Schmidt, and R. Aris, "Kinetics of Faceting of Crystals in Growth, Etching, and Equilibrium," *Phys. Rev. B*, **47**, 4896 (1993).

Westmoreland, P. R., and K. R. Cox, "Computational Chemistry and Its Industrial Applications," *AIChE Meeting*, San Francisco (1994).

Ziff, R. M., E. Gulari, and Y. Barshad, "Kinetic Phase Transitions in an Irreversible Surface-Reaction Model," *Phys. Rev. Lett.*, **56**(24), 2553 (1986).

Manuscript received Apr. 1, 1997, and revision received June 30, 1997.